WILEY | Hindawi

Research Article

The Spatiotemporal Characteristics of Coupling Effect between Roof and Backfill Body in Dense Backfill Mining

Xinyuan Zhao [ID],[1] **Xinwang Li,**[2] **Ke Yang** [ID],[1] **and Zhen Wei** [ID][1]

[1]*School of Mining Engineering, Anhui University of Science and Technology, Huainan 232001, China*
[2]*School of Mining and Geomatics, Hebei University of Engineering, Handan 056038, China*

Correspondence should be addressed to Ke Yang; keyang2003@163.com

Backfill mining has become an important part of coal mine green mining technology. In this paper, the spatiotemporal characteristics of coupling effect between the roof and dense backfill body were analyzed by theoretical analysis and similar simulation test, and Xingtai Mine in China was taken as an engineering case for verification. The results show that the larger subsidence of the roof is, the stronger the supporting capacity of the backfill body is, and the interaction between the two is more obvious, thus showing a coupling effect. This coupling effect presents a regular variation with the increase of backfill distance and time, that is, the coupling degree of roof and backfill body is high in the middle of goaf and low in the vicinity of the coal pillar in spatial distribution, and the coupling behavior of roof and backfill body continues to occur slowly with time. Through the monitoring of stress and displacement in the engineering site and the analysis of borehole observation results, the spatiotemporal coupling effect between roof subsidence and backfill support is fully verified. The research results are of great significance to the control of surrounding rock in backfill mining, the study of the mechanical aging characteristics of backfilling materials, and the optimization of backfill body support performance.

1. Introduction

Solid waste backfill mining technology has become an important content of green mine construction in recent years and is one of the four key technologies in the green mining technology system [1, 2]. Its main method is to fill the solid waste discharged in the process of coal production and utilization, such as gangue, and fly ash, into the underground goaf to achieve the purpose of replacing coal and digesting solid waste. This method plays an important role in controlling overburden deformation, reducing surface subsidence, and protecting the ecological environment [3–5].

At present, the research on solid waste backfill mining technology mainly focuses on two major aspects: strata control theory and backfilling material mechanical properties. In view of the research on the strata control theory of backfill mining, Zhang et al. [6, 7] studied the deformation characteristics of key stratum under the condition of comprehensive mechanized solid backfill mining by the elastic foundation beam theory and analyzed the influence of lithology of lower strata and backfilling materials on elastic foundation coefficient and the quantitative relationship between them; Liu et al. [8, 9] put forward the continuous curved beam model of overlying strata in dense backfill mining, elaborated the formation conditions and mechanical characteristics of continuous curved beam, and studied the space-time characteristics of continuous curved beam; Wang et al. [10] studied the movement law of overlying strata in longwall backfill panel and revealed the movement and deformation characteristics of immediate roof and main roof. On the basis of comprehensive analysis of strata movement and mechanical characteristics of backfill body, Chang et al. [11] established a mechanical model of rock beam in backfill mining by the theory of elastic foundation beam and analyzed the main influencing factors of strata movement and deformation; Li et al. [12] established a mechanical model of backfill body and roof in solid dense backfill mining by the theory of nonlinear elastic foundation of thin plate and analyzed the deflection equation of the roof by the energy method, derived the conditions of roof breakage; Fan et al. [13] proposed three

types of structures in the overburden under the backfill conditions based on the movement law of the overlying strata and established a mechanical model to derive the theoretical formula of the main roof subsidence. In addition, some scholars [14–19] have studied the movement law of overlying strata in backfill mining from different aspects. Study on the mechanical properties of solid backfilling materials, scholars mainly focused on the particle size, gradation [20, 21], deformation characteristics [22, 23], compaction characteristics [24–26], failure characteristics [27–29], acoustic emission characteristics of gangue materials [26], and the mechanical properties of solid backfill bodies and had obtained rich research results [30–36]. Under the condition of dense backfill, the ground pressure behaviors of the stope and the mechanical properties of the backfill body are not isolated, respectively; there must be an interaction between roof subsidence and backfill body support, which presents a spatiotemporal coupling relationship. However, there is little research on this topic.

In this paper, the interaction model between roof and backfill body was established. Based on the spatiotemporal evolution of ground pressure in backfill mining, the spatiotemporal distribution characteristics of the coupling law between roof and backfill body were analyzed, which were verified by similar material simulation experiments and engineering cases. The research results are of great significance to the control of surrounding rock in backfill mining, the study of the mechanical aging characteristics of backfilling materials, and the optimization of backfill body support performance.

2. Coupling Effect of Roof and Backfill Body

2.1. Coupling Analysis of Roof and Backfill Body with Different Goaf Backfilled Ratio. On the one hand, the goaf backfilled ratio reflects the compactness of the backfill body; on the other hand, it also affects the coupling behavior between the roof and backfill body [37]. The compactness of the backfill body in the goaf is different, and the coupling degree between the roof and the backfill body is also different, as shown in Figure 1.

When the goaf backfill body cannot reach the compacted state, there is a large gap between the backfill body and the immediate roof. The roof first compresses the gap between the backfill body and roof at the initial stage of bending and subsidence and then compresses the backfill body. During this process, the resistance of the backfill body to the roof is gradually enhanced. However, due to the large load of overburden and the large deflection of the roof subsidence, the initiation, development, expansion, and even penetration of the roof cracks cannot be prevented. If the goaf backfilled ratio is very low, the low position strata such as the immediate roof and the main roof will be broken at first.

When the goaf backfilled ratio is very high and a dense state is achieved, the backfill body can be regarded as basically in contact with the roof. Once the immediate roof is bent and subsided, it will contact with the backfill body. After that, the backfill body begins to produce the initial

supporting effect on the subsidence of the immediate roof. As the expansion of the goaf, the overburden load increases, the immediate roof bending degree increases. The dense backfill body has increasingly stronger resistance to the subsidence of the overburden and until the compression of the backfill body and the subsidence of the roof tend to balance. In this case, the roof has a small subsidence amount, and the degree of damage is small. Even the low position strata only produce partial nonpenetrating fractures, and the main roof maintains good integrity and stability and forms a continuous curved beam structure under certain conditions [38].

In summary, under the condition of dense backfill in goaf, the compactness and initial supporting force of the backfill body are higher, and the initial subsidence activity of the immediate roof will be restricted. The backfill body bears part of the overburden load, reduces the stress of hydraulic support in the backfill panel, and relieves the degree of ground pressure behavior in the stope, which is conducive to the subsequent dense backfill work and forms a benign cycle of dense backfill operation. So there is a coupling relationship between the dense backfill body and overlying strata. In addition, a large number of engineering practices and experimental studies show that the coupling effect of backfill body support and roof subsidence presents a spatiotemporal evolution characteristic with the advancement of the backfill panel, that is, the farther away from the backfill panel, the longer the time for the material to be filled into the goaf, the closer the overburden load and the backfill body resistance is to the relative equilibrium state. The distance between the goaf backfill body and the backfill panel also reflects the temporality of backfill advance, that is, the closer the distance is from the backfill panel, the shorter the time for the backfill body to be filled into the goaf, the lower the strength of the backfill body, the more unable to resist the roof subsidence, resulting in active roof subsidence and obvious ground pressure behavior. Therefore, from the backfill panel to the deep part of the goaf, there are active and stable periods of roof subsidence. Correspondingly, the enhancement area and compaction area of the backfill body are formed, as shown in Figure 2.

2.2. Spatiotemporal Coupling Effect of the Roof and Dense Backfill Body. When the goaf is densely filled, the immediate roof of the goaf is basically in contact with the dense backfill body, which can be approximately regarded as the roof subsidence amount equal to the compression amount of the backfill body. The coupling mechanical model of the roof and the backfill body is established, as shown in Figure 3.

In the stress concentration area of the coal seam in front of the backfill panel, there is

$$k_1(q_n)_1 = q_s, \tag{1}$$

where k_1 is the stress concentration factor and q_s is the supporting force of the coal seam.

It is assumed that some strata above the immediate roof will subside synchronously in dense backfill mining.
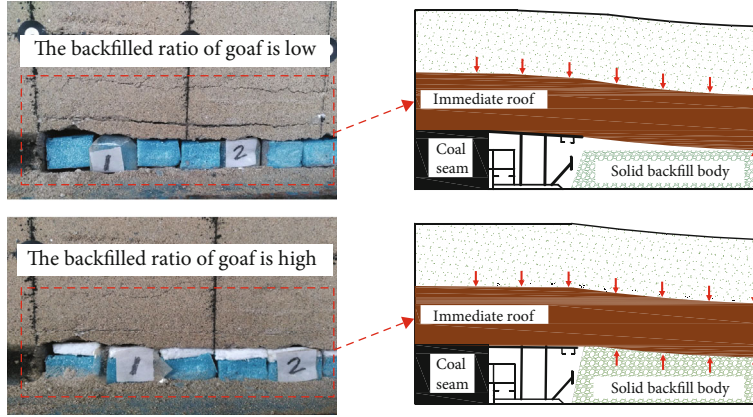
FIGURE 1: Schematic diagram of roof deformation with different backfilled ratios.
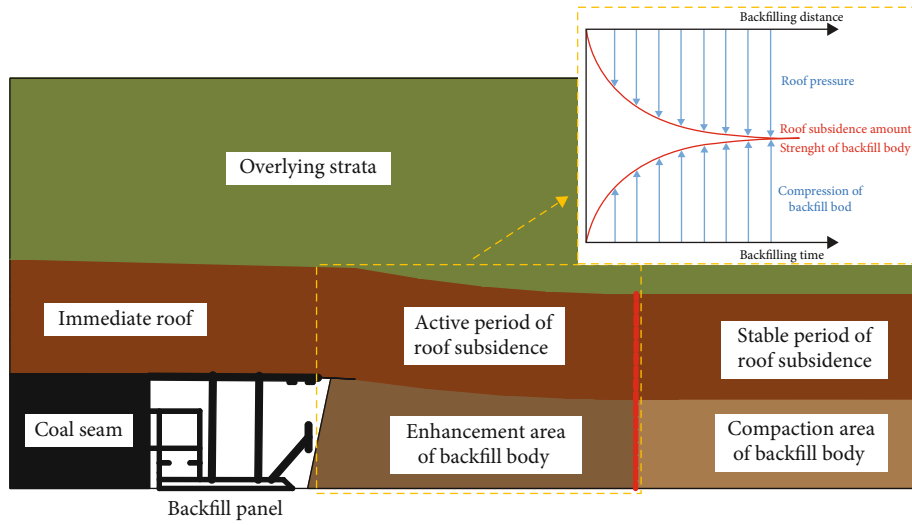

FIGURE 2: Schematic diagram of spatiotemporal coupling between the roof and the dense backfill body.
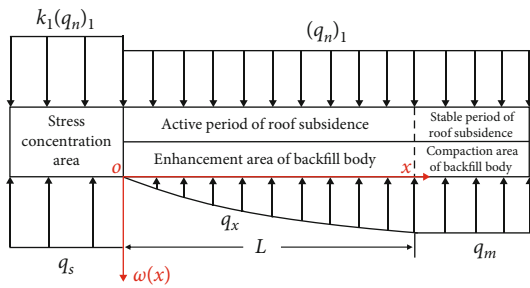

FIGURE 3: Coupling mechanical model of roof and backfill body.

According to the principle of composite beams [39], the load on the immediate roof is the load of the overlying n layers strata $(q_n)_1$, namely

$$(q_n)_1 = \frac{E_1 I_1 \sum_{i=1}^{n} \gamma_i h_i}{\sum_{i=1}^{n} E_i h_i^3}, \tag{2}$$

where E_1 and I_1 are the elastic modulus and moment of inertia of the immediate roof, respectively, and E_i, I_i, h_i,

and γ_i are the elastic modulus, the moment of inertia, thickness, and bulk density of the i-th layer, respectively.

From the backfill panel to the goaf, roof subsidence activity is gradually violent, and the supporting force of the backfill body gradually increases, until the two tend to be relatively balanced. Assuming that the length of the enhancement area of the backfill body is L, according to the elastic foundation theory [40], the deflection equation of the roof subsidence at this stage ($x < L$) is:

$$E_1 I_1 \frac{d^4 \omega(x)}{dx^4} + k\omega(x) = (q_n)_1, \tag{3}$$

where k is the coefficient of elastic foundation and x is the distance between the backfill body and the backfill panel.

Substitute $\alpha = \sqrt[4]{k/4E_1 I_1}$ into the above equation (3),

$$\omega(x) = \frac{(q_n)_1}{k} + e^{-\alpha x}((d_1 \cos(\alpha x) + d_2 \sin(\alpha x)) + e^{\alpha x}((d_3 \cos(\alpha x) + d_4 \sin(\alpha x)), \tag{4}$$
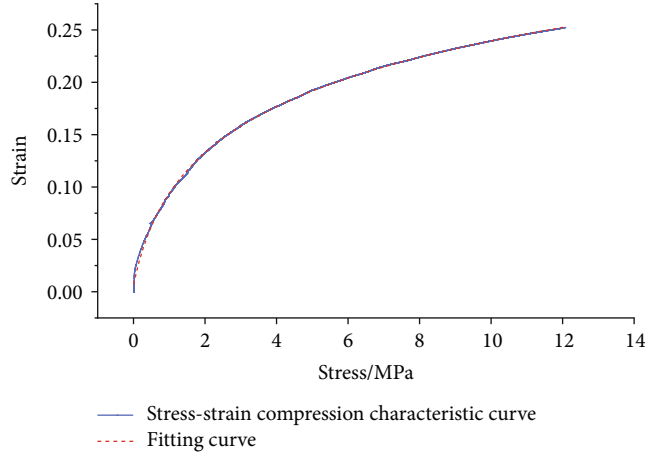
FIGURE 4: Compression fitting curve of backfilling material.

where d_1, d_2, d_3, and d_4 are the constant; it can be obtained from the boundary conditions.

Under the condition of dense backfill, the maximum subsidence deflection of the immediate roof in the backfilling area is equal to the maximum compression amount of backfill body under that load. Through the compression test of solid backfilling material, the compression characteristic curve of backfilling material is as shown in Figure 4 (stress $\sigma \leq 13$ MPa).

According to the fitting curve, the relationship between stress σ and strain ε of backfilling material can be expressed as follows:

$$\varepsilon = a \ln (\sigma + c) + b, \tag{5}$$

where a, b, and c are constants.

When $\sigma = q_x$, the subsidence deflection of the immediate roof at a certain position behind the backfill panel can be expressed as follows:

$$\omega(x) = \varepsilon h = ah \ln (q_x + c) + bh, \tag{6}$$

where q_x is the supporting force of the backfill body at a certain position behind the backfill panel.

The distance between the backfill body and backfill panel can be expressed by advancing days and daily advancing distance of the backfill panel, namely,

$$x = lt, \tag{7}$$

where l is the daily advance distance of the backfill panel and t is the number of days used when the backfill panel advances a certain distance. Substitute equation (7) into equation (6) to get:

$$\omega(lt) = ah \ln (q_x + c) + bh. \tag{8}$$

Equation (8) is the roof subsidence deflection at any position in the enhancement area of the backfill body.

When $x \geq L$, the compression of the backfill body and the subsidence of the roof are basically balanced, and the pressure on the backfill body is the load of the n layers of overlying strata, that is, $q_m = (q_n)_1$. The compression amount of backfill body and the roof subsidence amount also reach the maximum, namely,

$$\omega(L) = ah \ln ((q_n)_1 + c) + bh. \tag{9}$$

In the case of a certain mining height, there is a highly matched spatiotemporal coupling relationship between the subsidence deflection of the roof and the support strength of the backfill body, that is, the strength of the backfill body in different time and space reflects the degree of roof subsidence and ground pressure behavior in the corresponding time and space, and the subsidence deflection of the roof in different time and space reflects the strength of the backfill body in the corresponding time and space to a certain extent.

3. Engineering Background

This study takes the 7606 backfill panel of Xingtai Mine in China as the engineering background [41]. Xingtai Mine is located in the southwest of Xingtai City. The corresponding ground location of the 7606 backfill panel is the northwest of the Xingtai Mine industrial square (as shown in Figure 5). The special railway transportation line for the mining area passes above the backfill panel, and the south of the backfill panel is workshops and dormitories. The backfill panel is inside the protective coal pillar line of the industrial square, and its underground location is in the east of the mining area; the northeast is the goaf, the northwest is the fault, the south is 50 m away from the west main roadway, and the east is about 100 m away from the shaft station.

The coal seam where the backfill panel is located is 2# coal, which is a complex structure coal seam with an average inclination angle of 9° and an average buried depth of 320 m. The middle part of the coal seam contains a layer of 0.4 m thick gangue. The spontaneous combustion period of coal seams exceeds 12 months, the gas emission is small, and the ground temperature and pressure are normal. The average mining height of the backfill panel is about 3 m; the inclined length is 50 m. The immediate roof of the backfill
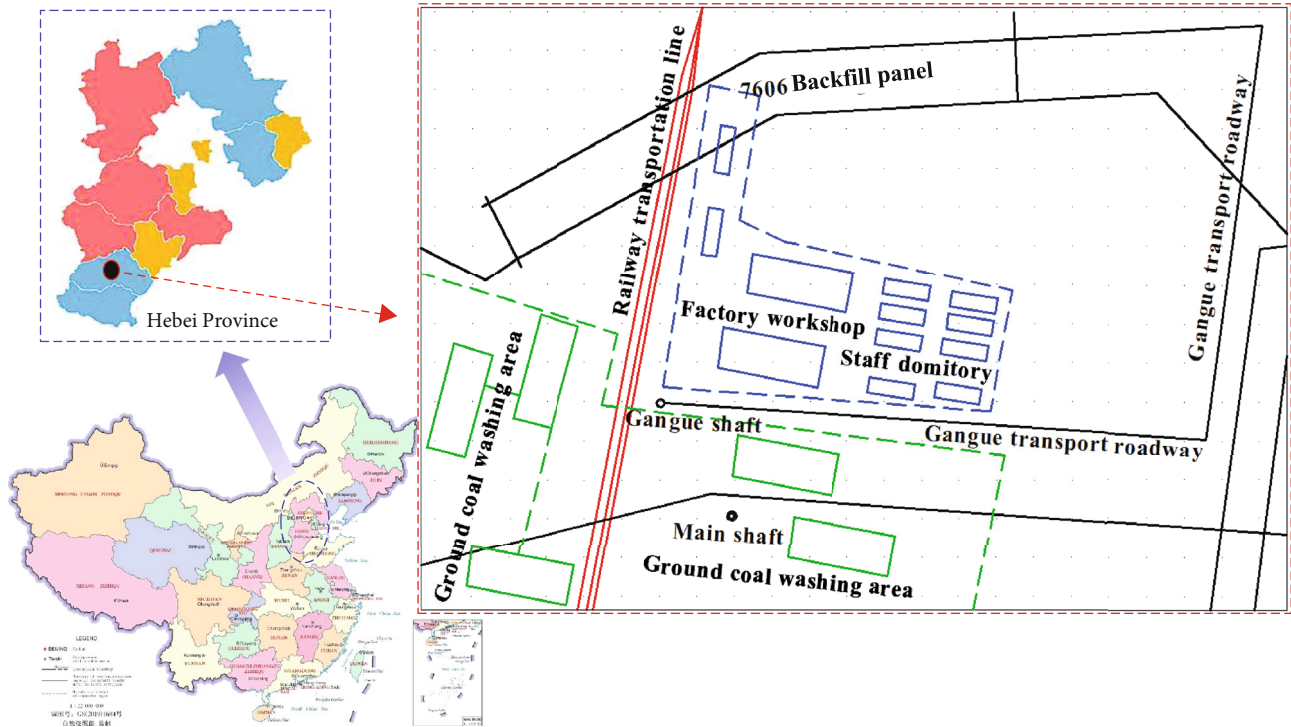
FIGURE 5: Location of backfill panel.

panel is sandy shale with an average thickness of 4.5 m, black, mainly muddy, and the main roof is fine sandstone. The local strata columnar diagram of the backfill panel is shown in Figure 6.

4. Physical Simulation Test

4.1. Model Parameters. According to the engineering background and laboratory conditions, the geometric similarity ratio of the model is determined to be 1 : 100 (model : prototype), the bulk weight similarity ratio is 1 : 1.6, and the stress similarity ratio is 1 : 160. The size of the physical simulation platform is 1.5 m × 0.1 m × 0.85 m (length × width × height), and a 0.04 MPa compensation load is applied to the upper part of the model to simulate unpaved rock stratum. Through laboratory sampling tests and consulting the relevant data of the mine, the material ratio and thickness of the rock stratum are shown in Table 1.

4.2. Selection of Similar Materials for Backfill Blocks. To more truly reflect the deformation law of overlying strata during solid backfill mining, according to the similarity principle, the compression characteristic curve of the simulated backfill body should be similar to that of the actual backfill body, so as to ensure the accuracy of dynamic deformation of similar simulation materials in the process of model excavation and backfilling. Combined with laboratory conditions, four kinds of soft and hard foam material groups with different thickness ratios were selected to carry out compression experiments to find suitable backfill body similar materials. Four kinds of material groups of soft and hard foams with different thickness ratios are, respectively, No. 1 material group with

soft foam : hard foam = 0 : 1, No. 2 material group with soft foam : hard foam = 1 : 0, No. 3 material group with soft foam : hard foam = 1 : 2, and No. 4 material group with soft foam : hard foam = 1 : 3. The composition of the four material groups and their compression curves are shown in Figure 7.

By comparing the compression characteristic curves of the four kinds of material groups with that of theoretical materials, No. 1 material group and No. 3 material group occur larger strain under the action of test force; the initial deformation of No. 2 material group is small, but as the test force increases, the deformation amount of No. 2 material group begins to increase rapidly. The above three material groups cannot be used as similar simulation materials for the backfill body because of the large strain during the compression process or the large difference between their compression curve trend and that of the theoretical material. The compression characteristic curve of No. 4 material group is very close to that of the theoretical material, so No. 4 material group is selected as the similar material of the simulated backfill body in this experiment, that is, the materials group of the backfill block is soft foam : hard foam = 1 : 3.

4.3. Simulation Scheme. In the process of modeling, a micropressure sensor is arranged at every 10 cm interval in the rock stratum about 5 cm above the coal seam, which are, respectively, numbered "R1-R10." Before the model is excavated and backfilled, it is necessary to apply a compensation load to the upper part of the model and balance the model. 20 cm coal pillars are reserved on both sides of the model, and 110 cm in the middle is the excavation and backfilling range.
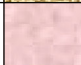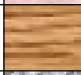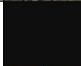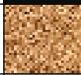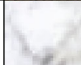
Layer number	Name of rock stratum	Bar chart	Lithology description
1	Sandy shale		Light gray, containing a lot of plant fossil fragments.
2	Medium sandstone		Light gray, mainly composed of quartz feldspar, clear bedding.
3	Sandy shale		Gray-black, containing plant fossils, partially containing bauxite.
4	Fine sandstone		Gray, with mica, clay cement.
5	Sandy shale		Black, with plant fossils, and a lot of mud.
6	Coal seam where the working face is		Black powder, good coal quality, containing plant fossils.
7	Sandy shale		Dark gray, thin layer, rich in plant fossils, mainly muddy, with squeezed bottom.
8	Fine sandstone		Gray, hard, horizontally layered.

FIGURE 6: Columnar diagram of local strata in the backfill panel.

TABLE 1: Material ratio of rock stratum in model.

Serial number	Strata name	Strata thickness/cm	Fine sand/kg	Lime/kg	Plaster/kg	Water/ml
1	Fine sandstone	4	9	0.64	0.64	1028
2	Sandy shale	6	12.5	0.42	0.42	1334
3	Coal seam	3	8	0.7	0.3	900
4	Sandy shale	4	9	0.56	0.56	1012
5	Fine sandstone	9	21	1.5	1.5	2400
6	Sandy shale	7	17	1.49	0.64	1913
7	Medium sandstone	6	14	1.17	1.17	1634
8	Sandy shale	8	18	1.13	1.13	2026
9	Coarse-grained sandstone	12	28	2	2	3200
10	Fine-grained sandstone	10	23	1.44	1.44	2588
11	Carbonaceous shale	6	12.5	0.69	0.69	1388
12	Fine sandstone	8	18	1.29	1.29	2058

According to the on-site backfilled ratio and daily advance distance, the average height of the block is set at 3 cm, and the average width is set at 3.3 cm, that is, about 3.3 cm of excavation is backfilled with one backfill block. For every three blocks backfilled, a pressure sensor is arranged in the middle backfill block to measure the stress of the backfill body. The backfill bodies with pressure sensors are numbered "ct1-ct11." In this experiment, each backfill block represents the daily backfill distance on-site, the whole process from model excavation, backfilling a block to balance takes 15 minutes, which is a backfilling time step. Step 34-37 is the standing stage after the completion of model excavation and backfilling. According to the on-site backfilling process, the coal seam is excavated 3.3 cm and backfilled with a backfill block. After the model is balanced, the next step of excavation and backfilling can be carried out and follow this cycle until the stopping line. In this process, the Donghua

Test DH3815N static strain testing system was used for collecting data regularly, and the time interval was 5 s. The XJTUDP three-dimensional photogrammetry system camera was used to take pictures every 10 cm of backfilling. After the excavation and backfilling of the model was completed, the collecting data was stopped, the model was left to stand for 12 hours, and then, three-dimensional photography was taken to observe the movement law of overburden. The specific layout of the pressure sensor is shown in Figure 8.

4.4. Spatiotemporal Coupling of Stress between Roof and Backfill Body. To clearly show the spatiotemporal coupling effect of roof and backfill body in stress, the stress data of roof measuring points numbered "R1, R3, R5, R7" and adjacent backfill body measuring points numbered "ct2, ct4, ct6, ct8" are as shown in Figure 9.
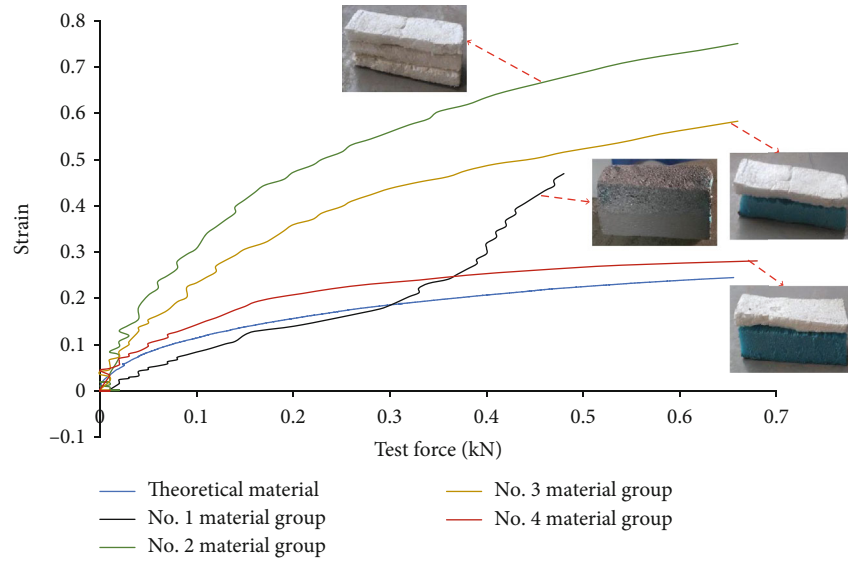
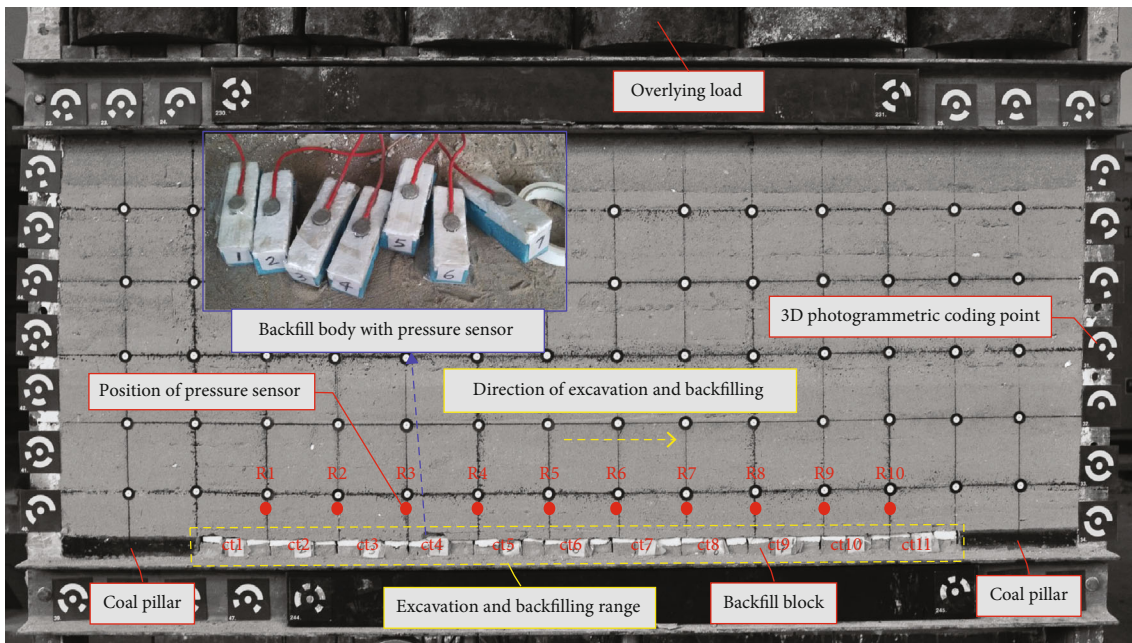FIGURE 7: Compression curves of different material groups.

FIGURE 8: Layout of model measuring points.

As seen from Figure 9, when the backfill panel is close to the measuring points R1, R3, R5, and R7, the corresponding measuring point stresses are 40 kPa, 45 kPa, 53 kPa, and 62 kPa, respectively, indicating that with the increase of the backfilling time step, the range of excavation and backfilling expands, and the peak of the concentrated stress in front of the backfill panel shows an increasing trend. After the backfill panel passes through the measuring points, the stress of each measuring point decreases sharply and then recovers slowly. The stress of the backfill body begins to increase slowly due to the roof compression, and the monitoring stress of the roof and backfill body gradually tends to be consistent. In the whole process of excavation and backfilling, the stress of the roof measuring point has experienced the variation process of stable increase-sharp decline-slow recovery, and the monitoring stress of the corresponding backfill body shows a slow increase-gradually stable variation law. The reason is that the front of the backfill panel is in the stress concentration area within a certain distance, and once the backfill panel passes through the roof measuring points, the immediate roof will subside and slightly separated from the main roof, resulting in rapid release of the stress at the roof measuring point. After 2-4 backfilling time steps, the subsidence degree of overlying strata increases; the roof contacts
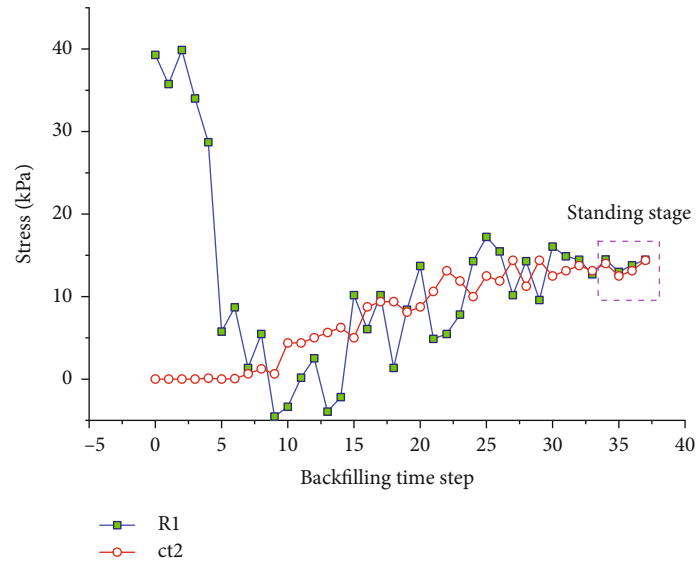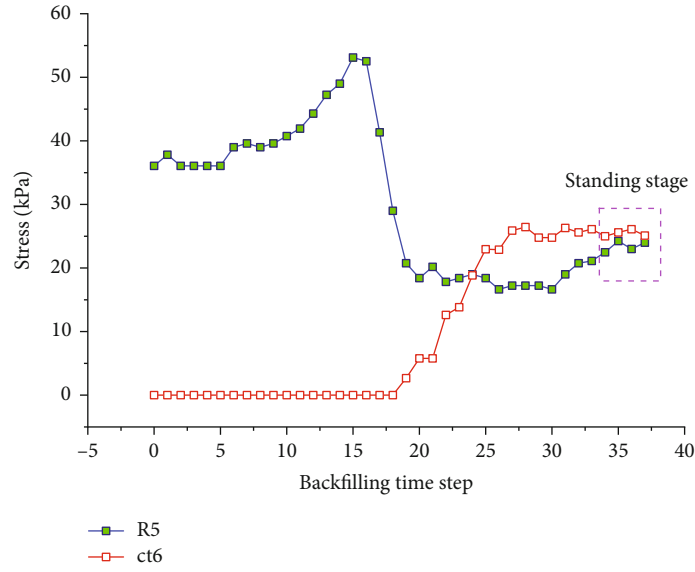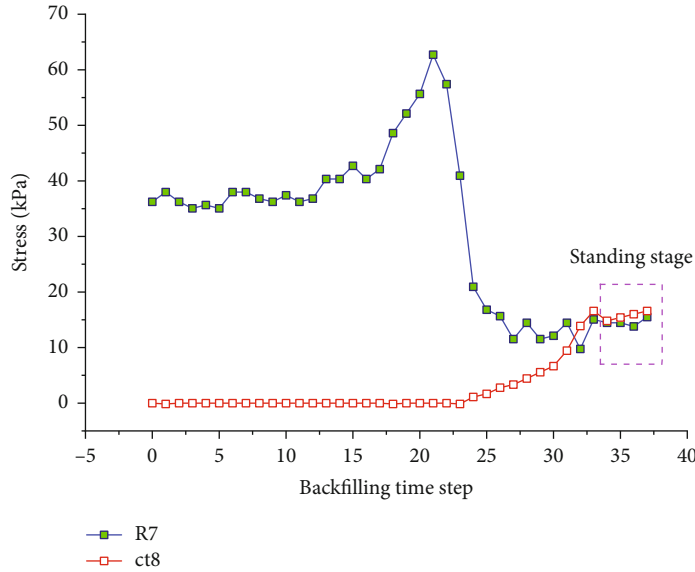
(a) Measuring points R1 and ct2
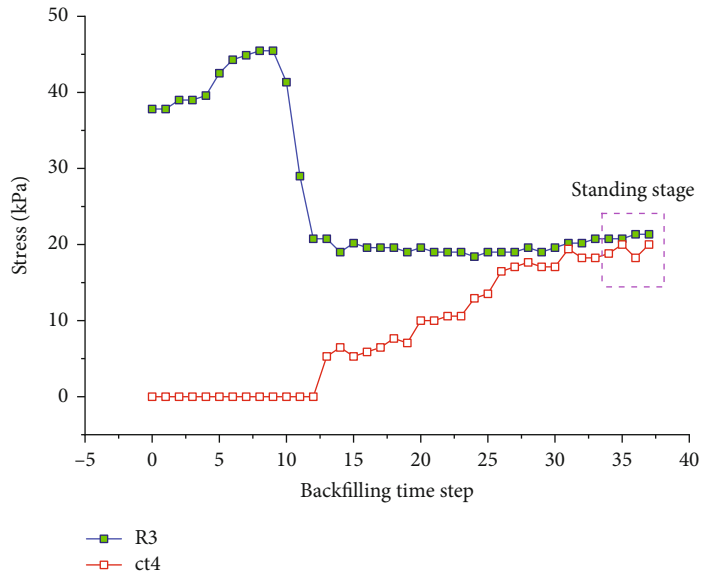
(b) Measuring points R3 and ct4

Figure 9: Continued.

(c) Measuring points R5 and ct6

(d) Measuring points R7 and ct8

FIGURE 9: Stress variation diagram of representative measuring points.

and compresses the backfill body, which causes the backfill body to generate support for the roof. The roof and the backfill body begin to have a coupling effect.

As the backfill panel continues to advance, the range of deformation and subsidence of the overlying strata increases. Under the interaction action of overburden load and backfill support, the delamination in the low roof is closed, and the stress of the roof measuring point slowly recovers, accompanied by the growth of the support stress of the backfill body. The stresses of the measuring points on the roof and the backfill body at the same position gradually approached, and they tend to be consistent after the backfill panel passes through the roof measuring points by 12-18 backfilling time steps. The coupling effect of roof and backfill body tends to be stable gradually. The monitoring stress of the roof and

backfill body is stable between 15 kPa and 25 kPa. The stress of R5/ct6 measuring point is larger than that of R1/ct2 measuring point after stabilization. The stress distribution of roof and backfill body is high in the middle of goaf and low in the vicinity of the coal pillar, which indicates that overburden subsidence and backfill compression are obvious in the middle of the excavation and backfilling range, and the coupling degree between the roof and backfill body is relatively high. The above analysis fully shows the spatiotemporal coupling effect of roof subsidence and backfill support in stress during the advancing process of the backfill panel.

4.5. Spatiotemporal Coupling of Displacement between Roof and Backfill Body. To show the spatiotemporal coupling characteristics of the roof and backfill body in displacement,

(a) Before excavation and backfilling

(b) The backfill distance is 20 m

(c) The backfill distance is 40 m

(d) The backfill distance is 60 m

(e) The backfill distance is 80 m

(f) The backfill distance is 100 m

(g) The backfill distance is 110 m

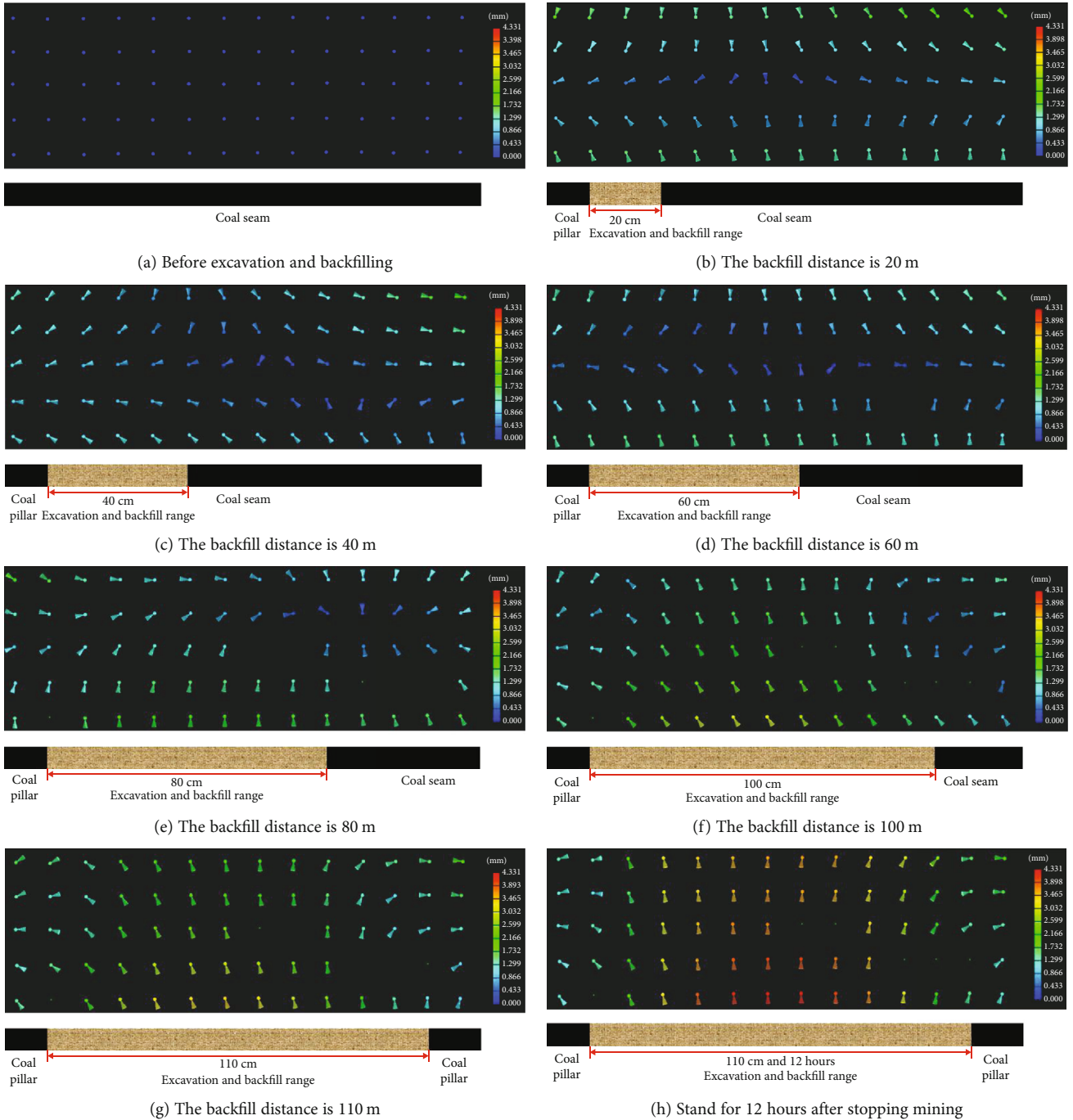(h) Stand for 12 hours after stopping mining

FIGURE 10: Deformation diagram of overlying strata during the backfill process.

the three-dimensional dynamic deformation diagram of the model during the excavation and backfilling process is as shown in Figure 10.

As can be seen from Figures 10(a)–10(g) that during the excavation and backfilling process, the overburden in front of the backfill panel is slightly deformed due to mining disturbance, and the overburden behind the backfill panel has a large amount of subsidence. Among them, the maximum subsidences of the roof after backfill 40 cm, 80 cm, and 110 cm are 1.299 mm, 2.166 mm, and 3.465 mm, respectively,

which indicates that the backfill distance increases, bending and subsidence of the roof in goaf are gradually obvious, the compression amount of backfill body increases gradually, and the interaction degree between them is higher. When the backfill distance is constant, from the top to the bottom of the roof and from the coal pillars on both sides to the goaf, the amount of roof subsidence shows an increasing trend. The area with the largest amount of roof subsidence is located in the middle of goaf, the roof subsidence in the vicinity of the coal pillar is small due to the support of the coal pillar,
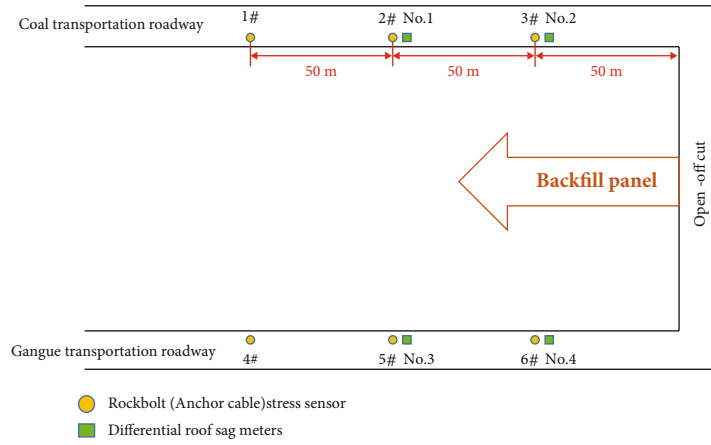
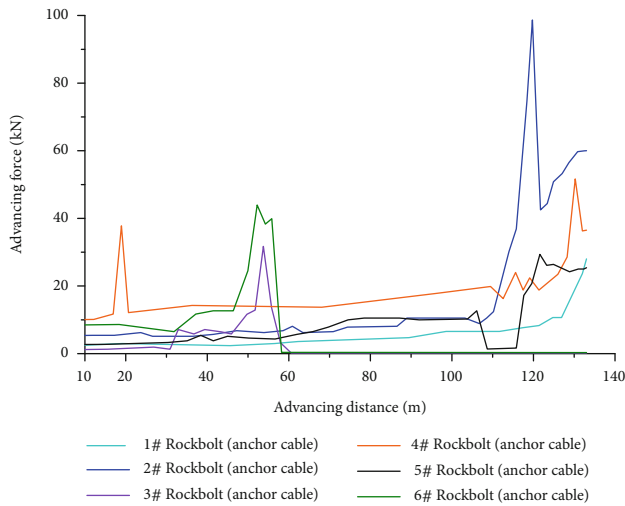FIGURE 11: Sensor layout in engineering site.

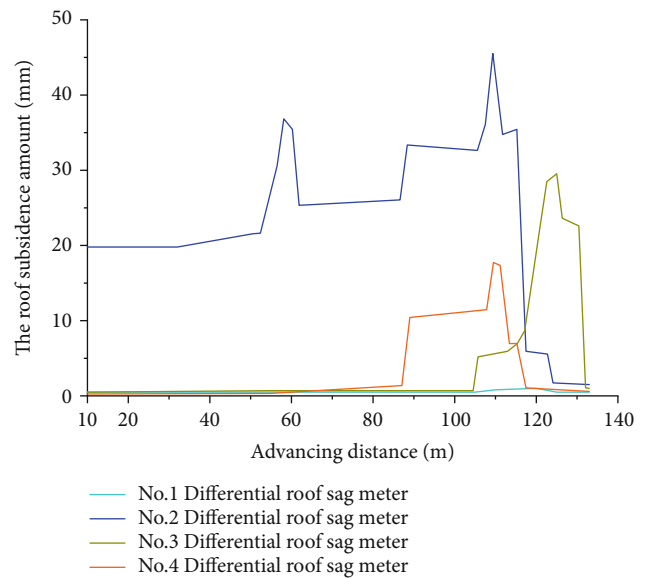FIGURE 12: Anchor force variation diagram of rockbolts (anchor cables).

FIGURE 13: Variation of roof bedding separation.

and the compression degree of the corresponding backfill body also shows the variation law of a large compression degree in the middle of goaf and the small in the vicinity of the coal pillar. The above results show that the coupling degree between the roof and the backfill body presents a spatial distribution of high in the middle of the goaf and low in the vicinity of the coal pillar, which is consistent with the stress coupling distribution law in Figure 5.

From the comparison of the deformation of the overlying strata in Figures 10(g) and 10(h), it is found that although the excavation and backfilling operation of the model has been completed, the deformation of the rock stratum has not stopped. At the same position of the model, the deformation of the overburden and the compression of the backfill body continues to increase slowly with time, indicating that the coupling behavior of the overburden subsidence and the backfill body supporting is still proceeding slowly and smoothly until the supporting force of the backfill body can resist the pressure of the roof subsidence.

5. Engineering Case Analysis

5.1. Layout of Monitoring Instruments. An industrial test of solid dense backfill was carried out at 7606 backfill panel of Xingtai Mine, China. In this test, the advance length of the backfill panel is about 133 m, the actual number of days used is about 40 days, the average daily advance distance is about 3.3 m, and the comprehensive mechanized solid dense backfill mining technology is adopted. To reflect the spatio-temporal coupling effect between the dense backfill body and the roof, according to the monitoring system design method [42], monitoring instruments are arranged in the stope and the backfill body, specifically: several hydraulic support pressure monitors are arranged along the inclination of the backfill panel, and a rockbolt (anchor cable) stress sensor and differential roof sag meters are arranged every 50 m in the upper and lower roadways of the backfill panel, with the numbers of "1#-6#" and "No.1-No.4" (as shown in Figure 11). The pressure sensor of the backfill body is
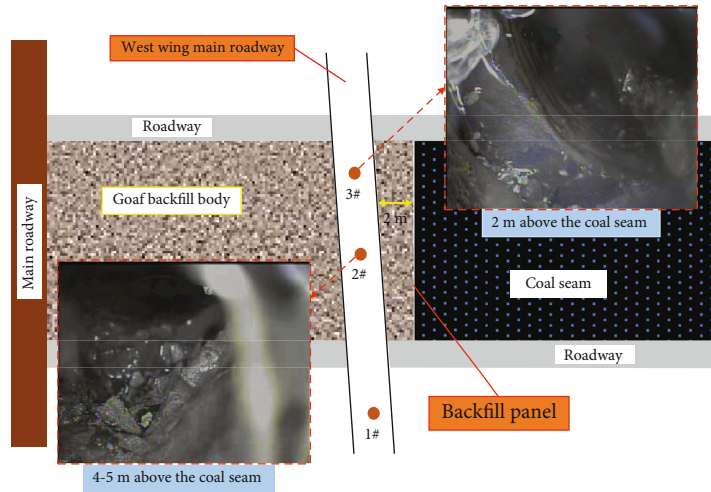
(a) The borehole is located 2 m behind the backfill panel
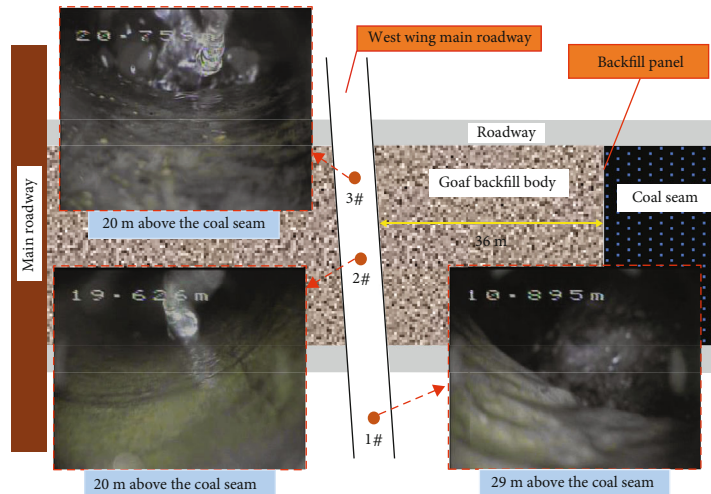
(b) The borehole is located 36 m behind the backfill panel

FIGURE 14: Borehole observation map.

arranged when the backfill panel is advanced 15 m, 40 m, and 65 m from the open-off cut.

5.2. Analysis of Monitoring Results.

The monitoring results of the working resistance of the hydraulic support show that the support pressure in the backfill panel is generally low, which is less than the rated working resistance. The initial pressure on the roof is not obvious, and the periodic weighting of the roof is weak. The periodic weighting step is between 40 and 55 m, indicating that the goaf backfill body can effectively control the movement of the overlying strata and weaken the ground pressure behavior of the stope.

As can be seen from Figure 12, when the rockbolts (anchor cables) are more than 50 m in front of the backfill panel, the variation of anchoring force is small, indicating that the mining impact of the backfill panel is small. The stress of 6# and 3# rockbolt (anchor cable) changes rapidly in the range of 50-60 m, which indicates that as the backfill panel advances, the rockbolts (anchor cables) gradually approach the backfill panel, and the anchoring force begins to increase. Within the scope of 20 m behind the backfill

panel, the anchoring force reaches the peak value, and the variation range is the largest, indicating that the roof subsidence near the stope is active and violent due to affected by mining behind the backfill panel. This stage corresponds to the active period of roof subsidence and the enhancement area of the backfill body in the above theoretical analysis. When the backfill panel is far away from the rockbolt (anchor cable) stress sensor, the anchoring force decreases rapidly and tends to be stable, which indicates that the roof subsidence activity tends to be stable at this stage; the roof subsidence and the backfill body support gradually reach a relative balance state.

As shown in Figure 13, the value of the differential roof sag meters changes little in front of the backfill panel due to less affected by mining. When the backfill panel is close to the differential roof sag meters, the amount of the roof bedding separation begins to increase, and when the differential roof sag meters are located 10-20 m behind the backfill panel, their value increases rapidly and reaches the peak value, indicating that the roof activity in this range is violent and the subsidence amount is large. When the No. 2 and No. 4

differential roof sag meters are located 50 m behind the backfill panel, their value increased significantly again, indicating that the roof appeared periodic weighting and severe subsidence occurred again. The results were basically consistent with the monitoring results of hydraulic support pressure in the backfill panel.

The pressure monitoring results of the backfill body show that the pressure is small in the range of 13-15 m behind the backfill panel; the maximum pressure is only 3.5 MPa, which indicates that part of the roof pressure is borne by the coal pillar. As it moves away from the backfill panel, the pressure of the backfill body gradually increases. The pressure of the backfill body reaches the maximum at a distance of 40 m from the backfill panel, which is 5.5 MPa. After that, the pressure of the backfill body is stable, and the roof subsidence and the compression of the backfill body gradually reach a basic balance.

5.3. Borehole Observation Results in the Overburden. In the -210 West Wing Main Roadway 40 m above the backfill panel, three detection boreholes are arranged along the inclination of the backfill panel, numbered 1#, 2#, and 3#, respectively.

As shown in Figure 14(a), when the -210 West Wing Main Roadway is located 2 m behind the backfill panel, the observation result of 2# borehole shows that the immediate roof and the main roof are separated at $4 \sim 5$ m above the goaf, broken locally, and there is water at the bottom of the hole; the observation results of 3# borehole show that there are local cracks at the immediate roof 2 m above the goaf. The above phenomena indicate that the immediate roof and the main roof only bend and subside due to the support of the backfill body at a short distance behind the backfill panel, and the coupling effect between the roof and the backfill body begins.

As can be seen from Figure 14(b), when the -210 West Wing Main Roadway is located 36 m behind the backfill panel, the observation result of 1# borehole shows local collapse occurs at about 29 m above the coal seam, and ponding occurs at about 23 m above the coal seam. The observation result of 2# borehole shows that local cracks appeared at 20 m above the coal seam and developed at 15 m above the coal seam. The observation result of 2# borehole shows that local cracks appeared at 20 m above the coal seam, and there was water at the bottom of the borehole. The above phenomenon shows that in the far distance behind the backfill panel, the strata fissures are gradually closed, the overburden subsidence and the backfill body support tend to be stable, the coupling behavior of the two becomes slow, and the coupling degree is high.

6. Conclusions

(1) The spatiotemporal coupling law of roof and backfill body in dense backfill mining is analyzed, and the mechanical coupling model of roof and backfill body is established. The spatiotemporal coupling relationship between roof subsidence deflection and support strength of the backfill body is quantitatively studied

(2) The analysis of the stress and deformation variation law of the roof and the backfill body obtained from the similar material simulation experiment shows that from the coal pillar to the goaf, the coupling degree of stress and displacement between roof and backfill body presents the spatial distribution of high in the middle of goaf and low in the vicinity of coal pillar. Moreover, the coupling behavior of roof subsidence and backfill body compression continues to occur slowly as time goes on after stopping mining, which reflects the time characteristics of coupling between roof and backfill body

(3) The industrial test of dense backfill in Xingtai Coal Mine of China is taken as an engineering case; the spatiotemporal coupling effect of the roof and backfill body in the backfill mining is studied and verified by the analysis of rockbolt (anchor cable) anchoring force, roof bedding separation amount, goaf backfill body stress, and borehole observation results

Data Availability

The data used to support the findings of this study are available from the corresponding author upon request.

Conflicts of Interest

The authors declare no conflict of interest.

Acknowledgments

References

[1] M. G. Qian, X. X. Miao, and J. L. Xu, "Green mining of coal resources harmonizing with environment," *Journal of China Coal Society*, vol. 32, no. 1, pp. 1–7, 2007.

[2] X. X. Miao and M. G. Qian, "Research on green mining of coal resources in China: current status and future prospects," *Journal of Mining & Safety Engineering*, vol. 26, no. 1, pp. 1–14, 2009.

[3] J. S. Hema, R. S. Kannan, and F. Z. Paul, "Use of waste materials for control of acid mine drainage and subsidence," *Journal of Environmental Engineering*, vol. 129, no. 10, pp. 910–915, 2003.

[4] T. Dutta, K.-H. Kim, M. Uchimiya et al., "Global demand for rare earth resources and strategies for green mining," *Environmental Research*, vol. 150, pp. 182–190, 2016.

[5] Z. G. Tao, C. Zhu, M. C. He, and M. Karakus, "A physical modeling-based study on the control mechanisms of Negative Poisson's ratio anchor cable on the stratified toppling deformation of anti-inclined slopes," *International Journal of Rock Mechanics and Mining Sciences*, vol. 138, p. 104632, 2021.

[6] J. X. Zhang, Q. Wu, Y. L. Huang, and Y. J. Zhou, "Strata pressure behavior by raw waste backfilling with fully mechanized

coal mining technology," *Journal of China Coal Society*, vol. 35, Supplement 1, pp. l–4, 2010.

[7] J. X. Zhang, J. Li, T. L. An, and Y. L. Huang, "Deformation characteristic of key stratum overburden by raw waste backfilling with fully-mechanized coal mining technology," *Journal of China Coal Society*, vol. 35, no. 3, pp. 357–362, 2010.

[8] J. G. Liu, J. W. Zhao, M. M. Li, and J. P. Zuo, "Continuous curved beam formation and strata control theory in coal backfill mining," *Journal of China Coal Society*, vol. 41, no. 2, pp. 383–391, 2016.

[9] J. G. Liu, J. W. Zhao, and H. Z. Yang, "Study on the time and space characteristics of continuous curved beam under backfill mining condition," *Coal Science and Technology*, vol. 45, no. 1, pp. 41–47, 2017.

[10] G.-C. Wang, S.-L. Yang, B.-G. Yang, and X. Wang, "Simulation experiment of overlying strata movement features of longwall with gangue backfill mining," *Journal of China Coal Society*, vol. 37, no. 8, pp. 1256–1262, 2012.

[11] Q. L. Chang, H. Q. Zhou, J. B. Bai, C. R. Duan, and Y. W. Li, "Stability study and practice of overlying strata with paste backfilling," *Journal of Mining & Safety Engineering*, vol. 28, no. 2, pp. 279–282, 2011.

[12] M. Li, J. Zhang, Z. Liu, X. Zhao, and P. Huang, "Mechanical analysis of roof stability under nonlinear compaction of solid backfill body," *International Journal of Mining Science and Technology*, vol. 26, no. 5, pp. 863–868, 2016.

[13] C. Fan, S. Li, L. Hai, W. Du, and Z. Yang, "Structure and deformation law of overlying strata for waste rock-fly ash backfilling mining," *Chinese Journal of Underground Space and Engineering*, vol. 14, no. 1, pp. 117–123, 2018.

[14] F. P. Hassani, A. Mortazavi, and M. Shabani, "An investigation of mechanisms involved in backfill-rock mass behaviour in narrow vein mining," *Journal of the Southern African Institute of Mining and Metallurgy*, vol. 108, no. 8, pp. 463–472, 2008.

[15] F. Ju, P. Huang, S. Guo, M. Xiao, and L. Lan, "A roof model and its application in solid backfilling mining," *International Journal of Mining Science and Technology*, vol. 27, no. 1, pp. 139–143, 2017.

[16] L. Wang, X. N. Zhang, G. L. Guo, and J. F. Cha, "Research on surface subsidence prediction model of coal mining with solid compacted backfill," *Rock and Soil Mechanics*, vol. 35, no. 7, pp. 1973–1978, 2014.

[17] Z. Li, S. Liu, W. Ren, J. Fang, Q. Zhu, and Z. Dun, "Multiscale laboratory study and numerical analysis of water-weakening effect on shale," *Advances in Materials Science and Engineering*, vol. 2020, Article ID 5263431, 14 pages, 2020.

[18] Y. L. Huang, *Ground Control Theory and Application of Solid Dense Backfill in Coal Mines, [Ph.D. thesis]*, China University of Min and Technol, Xuzhou, 2012.

[19] C. Zhu, M. C. He, M. Karakus, X. Cui, and Z. Tao, "Investigating toppling failure mechanism of anti-dip layered slope due to excavation by physical modelling," *Rock Mechanics and Rock Engineering*, vol. 53, no. 11, pp. 5029–5050, 2020.

[20] D.-l. Yang, J.-p. Li, C.-l. Du, K.-h. Zheng, and S.-y. Liu, "Particle size distribution of coal and gangue after impact-crush separation," *Journal of Central South University*, vol. 24, no. 6, pp. 1252–1262, 2017.

[21] M. Li, J. Zhang, Y. Huang, and N. Zhou, "Effects of particle size of crushed gangue backfill materials on surface subsidence and its application under buildings," *Environ Earth Science*, vol. 76, no. 17, p. 603, 2017.

[22] Y. N. Sun, P. S. Zhang, W. Yan, F.Q. Yan, and J. D. Wu, "Experimental study on pressure-bearing deformation characteristics of crushed sandstone in gob," *Coal Science and Technology*, vol. 47, no. 12, pp. 56–61, 2019.

[23] Z. G. Ma, G. L. Guo, R. H. Chen, and X. B. Mao, "An experimental study on the compaction of water-saturated overbroken rock," *Chinese Journal of Rock Mechanics and Engineering*, vol. 24, no. 7, pp. 1139–1144, 2005.

[24] B. N. Hu and A. G. Guo, "Testing study on coal waste back backfilling material compression simulation," *Journal of the China Coal Society*, vol. 34, no. 8, pp. 1076–1080, 2009.

[25] C. D. Su, M. Gu, X. Tang, and W. B. Guo, "Experiment study of compaction characteristics of crushed stones from coal seam roof," *Chinese Journal of Rock Mechanics and Engineering*, vol. 31, no. 1, pp. 18–26, 2012.

[26] M. M. Feng, J. Y. Wu, Z. Q. Chen, X. B. Mao, and B. Y. Yu, "Experimental study on the compaction of saturated broken rock of continuous gradation," *Journal of China Coal Society*, vol. 41, no. 9, pp. 2195–2202, 2016.

[27] Z. Li, H. X. Liu, Z. L. Dun, L. Ren, and J. Fang, "Grouting effect on rock fracture using shear and seepage assessment," *Construction and Building Materials*, vol. 242, p. 118131, 2020.

[28] Q. Meng, H. Wang, M. Cai, W. Xu, X. Zhuang, and T. Rabczuk, "Three-dimensional mesoscale computational modeling of soil-rock mixtures with concave particles," *Engineering Geology*, vol. 277, article 105802, 2020.

[29] Y. Wang, B. Zhang, S. H. Gao, and C. H. Li, "Investigation on the effect of freeze-thaw on fracture mode classification in marble subjected to multi-level cyclic loads," *Theoretical and Applied Fracture Mechanics*, vol. 111, article 102847, 2021.

[30] W. Li, Y. L. Huang, H. D. Gao, J. M. Li, and Z. Y. Ruan, "Study on acoustic emission characteristics of guague of different graduations during confined compression," *Journal of Mining and Safety Engineering*, vol. 37, no. 1, pp. 155–161, 2020.

[31] M. Zhou, Y. W. Dou, Y. Z. Zhang, Y. Zhang, and B. Zhang, "Effects of the variety and content of coal gangue coarse aggregate on the mechanical properties of concrete," *Construction and Building Materials*, vol. 220, pp. 386–395, 2019.

[32] C. Zhu, X. D. Xu, and W. R. Liu, "Softening damage analysis of gypsum rock with water immersion time based on laboratory experiment," *IEEE Access*, vol. 7, pp. 125575–125585, 2019.

[33] X. Du, G. Feng, T. Qi, Y. Guo, Y. Zhang, and Z. Wang, "Failure characteristics of large unconfined cemented gangue backfill structure in partial backfill mining," *Construction and Building Materials*, vol. 194, pp. 257–265, 2019.

[34] C. Zhu, M. C. He, Q. Yin, and X. H. Zhang, "Numerical simulation of rockfalls colliding with a gravel cushion with varying thicknesses and particle sizes," *Geomechanics and Geophysics for Geo-Energy and Geo-Resources*, vol. 7, no. 1, p. 11, 2021.

[35] D. W. Yin, S. J. Chen, Y. Ge, and R. Liu, "Mechanical properties of rock–coal bi-material samples with different lithologies under uniaxial loading," *Journal of Materials Research and Technology*, vol. 10, pp. 322–338, 2021.

[36] M. Li, J. X. Zhang, A. L. Li, and N. Zhou, "Reutilisation of coal gangue and fly ash as underground backfill materials for surface subsidence control," *Journal of Cleaner Production*, vol. 254, article 120113, 2020.

[37] Q. Zhang, J. Zhang, J. Wang, and P. Huang, "Theoretical research and its engineering practice on critical backfill ratio in backfill mining," *Journal of China Coal Society*, vol. 42, no. 12, pp. 3081–3088, 2017.

[38] J. P. Zuo, Y. B. Zhou, G. W. Liu, G. Y. Shao, and Y. Shi, "Continuous deformation law and curvature model of rock strata in coal backfill mining," *Rock and Soil Mechanics*, vol. 40, no. 3, pp. 1–9, 2019.

[39] M. G. Qian, P. W. Shi, and J. L. Xu, *Mine pressure and strata control*, China University of mining and Technology Press, Xuzhou, 2003.

[40] L. Yuqiu, *Calculation of Beams on the Elastic Foundation*, Beijing People's education press, Beijing, 1982.

[41] X. W. Li, X. Y. Zhao, L. C. Cheng et al., "Study on space-time evolution law of strata behaviors under dense backfill," *Chinese Journal of Rock Mechanics and Engineering*, vol. 39, no. 2, pp. 341–348, 2020.

[42] C. Zhu, Z. H. Yan, Y. Lin, F. Xiong, and Z. Tao, "Design and application of a monitoring system for a deep railway foundation pit project," *IEEE Access*, vol. 7, pp. 107591–107601, 2019.